CHALMERS
UNIVERSITY OF TECHNOLOGY

IMU-Based Posture Monitoring for Rehabilitation Applications

Master's thesis in Biomedical Engineering, MPMED

Yi Zhou

DEPARTMENT OFELECTRICAL ENGINEERING

CHALMERS UNIVERSITY OF TECHNOLOGY
Gothenburg, Sweden 2026
www.chalmers.se

Master's thesis 2026

IMU-Based Posture Monitoring for Rehabilitation Applications

Yi Zhou

CHALMERS
UNIVERSITY OF TECHNOLOGY

Department of Electrical Engineering
Division of Signal Processing and Biomedical Engineering
Chalmers University of Technology
Gothenburg, Sweden 2026

IMU-Based Posture Monitoring for Rehabilitation Applications
Yi Zhou

Supervisor: Xuezhi Zeng, Associate Professor at Division of Signal Processing and Biomedical Engineering, Electrical Engineering, Chalmers
Examiner: Xuezhi Zeng, Associate Professor at Division of Signal Processing and Biomedical Engineering, Electrical Engineering, Chalmers

Master's Thesis 2026
Department of Electrical Engineering
Division of Signal Processing and Biomedical Engineering
Chalmers University of Technology
SE-412 96 Gothenburg
Telephone +46 31 772 1000

Cover: An Xsens Movella DOT system consisting of five IMU sensors and the corresponding mobile application

Typeset in LaTeX
Printed by Chalmers Reproservice
Gothenburg, Sweden 2026

IMU-Based Posture Monitoring for Rehabilitation Applications
Yi Zhou
Department of Electrical Engineering
Chalmers University of Technology

Abstract

Accurate assessment of posture is important in rehabilitation-related applications, where abnormal body alignment may contribute to musculoskeletal discomfort, altered movement patterns, and reduced functional performance. Inertial Measurement Units (IMUs) provide a portable and low-cost alternative to laboratory-based motion capture systems for posture monitoring.

This thesis investigated the accuracy and reliability of IMU-based posture estimation using Movella DOT sensors, with a Qualisys optical motion capture (MoCap) system used as the reference measurement. Four sagittal posture variables were evaluated: pelvic tilt, thorax tilt, thorax–pelvis relative alignment, and forward head posture (FHP). The influence of breathing on thorax-mounted IMU measurements was investigated, and the feasibility of IMU-based respiration monitoring was also explored.

The results demonstrated good agreement between IMU-based posture estimates and the MoCap reference for pelvic tilt, thorax tilt, and thorax–pelvis alignment, with mean RMSE values of 0.86°, 1.65°, and 1.82°, respectively, and ICC values above 0.96 for all three variables. Forward head posture showed lower agreement and greater inter-subject variability. The comparison between Euler-angle–based and quaternion-based methods revealed only minor differences under the evaluated posture conditions. Deep breathing introduced visible oscillations and increased variability in thorax-mounted IMU signals, although overall IMU–MoCap agreement remained high. IMU-based respiration monitoring demonstrated moderate to strong agreement with a respiratory belt reference during deep breathing, but lower reliability during normal breathing.

Overall, the findings indicate that IMU-based sagittal posture estimation is feasible for rehabilitation-related posture monitoring, particularly for pelvic and thoracic measurements.

Keywords: IMU, Motion capture, rehabilitation, respiratory motion, wearable sensing

Acknowledgements

I would like to thank my examiner and supervisor, Dr. Xuezhi Zeng, for her continuous guidance, support, and encouragement throughout this thesis. I am deeply grateful for her patient supervision and responsible guidance, from which I have learned a great deal both academically and personally during this project.

I would also like to thank Tingting Zhao for her continuous encouragement and valuable advice throughout this work. I am especially grateful for her help in recruiting participants for the experiments.

Finally, I would like to express my heartfelt gratitude to my parents for their constant support, encouragement, and understanding throughout my studies.

Yi Zhou, Gothenburg, May 2026

List of Acronyms

Below is the list of acronyms that have been used throughout this thesis listed in alphabetical order:

EKF	Extended Kalman Filter
FHP	Forward Head Posture
ICC	Intraclass Correlation Coefficient
IMU	Inertial Measurement Unit
MEMS	Micro-Electromechanical Systems
MoCap	Motion Capture
RMSE	Root Mean Square Error
SD	Standard Deviation
STMA	Soft-Tissue Motion Artefact

Nomenclature

Below is the nomenclature of mathematical symbols used throughout this thesis.

θ	Sagittal tilt angle
θ_P	Pelvic tilt angle
θ_T	Thorax tilt angle
θ_{TP}	Thorax–pelvis relative alignment
θ_{FHP}	Forward head posture angle
θ_H	Head tilt angle
θ_{C7}	Cervical segment tilt angle
$\mathbf{R}$	Rotation matrix
$\mathbf{q}$	Quaternion
$\mathbf{q}_{\mathrm{rel}}$	Relative quaternion between chest and back sensors
r	Pearson correlation coefficient
R^2	Coefficient of determination
s	Sign correction factor
N	Number of valid samples

Contents

List of Figures

List of Tables

1
Introduction

1.1 Background

In modern daily life and working environments, musculoskeletal disorders are becoming increasingly common, particularly among individuals engaged in prolonged sitting or screen-based activities [1]. These conditions are often driven by poor postural habits and accompanied by muscular fatigue and reduced movement efficiency [2, 3]. Rehabilitation training is widely used to manage such disorders, with the aim of reducing pain, improving movement function, and supporting physical recovery [4, 5].

In rehabilitation-related settings, posture assessment is an important component because it provides information about body alignment, movement quality, and recovery progress [6]. From a biomechanical perspective, sagittal alignment of the pelvis, thorax, and cervical region is important for maintaining spinal curvature, balance control, and effective load transfer along the body axis [7]. Altered pelvic tilt, excessive thoracic inclination, and forward head posture may change the mechanical relationship between body segments and influence movement coordination [8, 9]. These parameters have each been associated with specific clinical consequences: anterior pelvic tilt with low back pain [10], excessive thoracic kyphosis with reduced respiratory function and shoulder impingement [11], and forward head posture with neck pain and cervical muscle dysfunction [12, 13]. Therefore, objective and reliable quantification of sagittal posture is essential for consistent rehabilitation evaluation and clinical decision-making.

However, the population requiring posture-related rehabilitation services has grown rapidly, while the number of professional therapists and institutions remains limited [14]. Traditional assessment methods based on clinical experience and manual measurements are often cumbersome, suffer from limited accuracy, and hinder long-term data management [15, 16]. Consequently, there is a strong need for objective and efficient posture monitoring technologies.

1.2 Related Work and Research Gap

Various methods have been developed for clinical and laboratory-based posture assessment, each with distinct advantages and limitations.

Visual inspection by physiotherapists or clinicians remains the most common method for posture assessment in routine clinical practice [17]. It requires no specialised equipment and can be performed rapidly in clinical settings. However, visual in-

spection is subjective and highly dependent on clinician experience, leading to significant intra- and inter-rater variability [15]. In addition, visual inspection does not provide quantitative results, which limits its use for long-term monitoring and documentation in rehabilitation.

Radiographic techniques, including standard X-ray and computed tomography (CT), are considered reference standards for assessing spinal curvature and segmental alignment [18]. Parameters such as lumbar lordosis, thoracic kyphosis, and sacral slope can be measured with high accuracy from lateral radiographs. However, radiation exposure, high cost, and the requirement for specialised facilities restrict their use to specific diagnostic contexts and prevent their application for routine or repeated posture monitoring during rehabilitation [18].

Optical motion capture (MoCap) systems using retroreflective markers and high-speed infrared cameras represent a laboratory gold standard for measuring body-segment kinematics [19]. These systems can provide sub-millimetre spatial resolution and high temporal accuracy, enabling detailed analysis of dynamic movement patterns. However, MoCap systems require expensive infrastructure, dedicated laboratory space, time-consuming marker placement, and technically skilled operators [19]. These constraints make MoCap impractical for routine clinical use and long-term rehabilitation monitoring outside controlled research environments.

Inertial Measurement Units (IMUs) have emerged as a practical alternative for posture monitoring in both laboratory and real-world settings. IMUs are portable, low-cost, and capable of continuous measurement without line-of-sight constraints [20]. Due to their small size, wireless capability, and suitability for wearable applications, IMUs have been increasingly used in human motion analysis, rehabilitation monitoring, and posture estimation [21, 22]. Seel et al. used IMUs to estimate joint flexion and extension angles, reporting an RMSE of less than 1° [23]. Zheng et al. developed a lower-limb kinematic model using IMUs for real-time full-body motion capture [24]. Paloschi et al. validated a wearable posture monitoring system based on magneto-inertial measurement units positioned along the spine to estimate thoracic kyphosis and lumbar lordosis [25]. Lee et al. investigated two commercially available IMU systems for upper-body posture monitoring during prolonged computer use [26]. A three-module IMU system was used to monitor spinal curvature changes during trunk movements, with root mean squared differences below 3.1° in the sagittal plane [27]. However, many studies focused on specific joints, selected spinal curvatures, or particular movement tasks, and few have provided a systematic evaluation across multiple sagittal posture variables simultaneously.

Despite the growing body of IMU-based posture research, several gaps remain. A systematic evaluation covering pelvic tilt, thorax tilt, thorax–pelvis alignment, and forward head posture, validated against a laboratory-grade MoCap reference system, is still lacking. Furthermore, the influence of breathing on IMU measurements has received limited attention, and the feasibility of using IMU signals for respiration monitoring has not been fully explored. Therefore, this thesis evaluates the accuracy and reliability of IMU-based sagittal posture estimation across these variables, examines how breathing affects thorax-mounted IMU measurements, and explores the feasibility of IMU-based respiration monitoring.

1.3 Aim and Research Objectives

1.3.1 Aim

The aim of this thesis is to develop and evaluate a reliable IMU-based method for sagittal posture assessment in rehabilitation-related applications.

- Quantify sagittal alignment parameters using IMUs, including pelvic tilt, thorax tilt, thorax–pelvis relative alignment, and forward head posture (FHP), to characterize multi-segment postural alignment.
- Compare Euler-angle–based and quaternion-based posture estimation methods and evaluate their influence on measurement stability and accuracy.
- Investigate the influence of respiratory movement on IMU-based posture estimation.
- Explore the feasibility of using IMU signals for respiration monitoring.

1.3.2 Research Questions

The main research question of this thesis is:

> How accurately and reliably can IMU-based systems quantify multi-segment sagittal posture across different posture tasks?

This question is investigated through the following sub-questions:

- How accurate and reliable is IMU-based estimation of sagittal alignment when evaluated using quantitative metrics such as RMSE, R^2, and ICC?
- How do different orientation estimation methods, including Euler-angle–based and quaternion-based approaches, influence posture estimation performance?
- How do respiratory movement influence the accuracy and repeatability of IMU-based posture estimation?
- Is it feasible to extract respiration-related information from IMU posture signals?

1.4 Scope and Limitations

This thesis focuses on the accuracy, reliability, and robustness of IMU-based sagittal posture estimation methods under experimental conditions. Several limitations should be noted from the outset.

First, the study included only four healthy adult participants. This small sample size limits the statistical power of the findings and the generalisability of the results to broader populations.

Second, all data processing was performed off-line after data collection. Real-time implementation of the proposed methods was not evaluated in this work.

Third, the study was restricted to healthy subjects under controlled laboratory conditions. The applicability of the methods to clinical rehabilitation populations with musculoskeletal conditions remains to be established.

Fourth, only sagittal-plane posture variables were evaluated. Multi-planar posture assessment was not addressed.

Finally, this thesis does not provide clinical interpretation of the results. The findings are evaluated in terms of measurement accuracy and agreement with a reference system, but no clinical conclusions regarding rehabilitation outcomes are drawn.

1.5 Thesis Structure

Chapter 2 presents the theoretical background related to sagittal posture biomechanics, IMU sensor principles, orientation estimation, and respiratory effects on IMU measurements.
Chapter 3 describes the experimental methods and is divided into two parts. Part A focuses on IMU-based sagittal posture estimation, including posture tasks, signal processing, and evaluation methods. Part B presents the experimental setup and processing methods for exploratory IMU-based respiration monitoring.
Chapter 4 presents the corresponding experimental results. Part A reports the accuracy and reliability of sagittal posture estimation, comparison of orientation estimation methods, and the influence of respiratory motion. Part B presents the results of the respiration monitoring feasibility analysis.
Chapter 5 discusses the findings, implications, and limitations of both parts of the study, followed by conclusions and suggestions for future work.

2
Theory

This chapter describes the theoretical background underlying the IMU-based posture estimation methods used in this thesis. It covers the working principles of IMU sensors, sensor fusion using the Kalman filter, and orientation representation methods including Euler angles and quaternions.

2.1 IMU Sensor Principles

An inertial measurement unit (IMU) typically integrates three types of micro electromechanical sensors (MEMS): a three-axis accelerometer, a three-axis gyroscope, and optionally a three-axis magnetometer [28]. Each sensor measures a different physical quantity and contributes complementary information to the overall orientation estimate.

2.1.1 Accelerometer

An accelerometer measures the specific force acting on the sensor, which includes both linear acceleration and the gravitational component. For a sensor at rest, the measured output reflects the direction of gravity:

$$\mathbf{a}_{\text{meas}} = \mathbf{a}_{\text{linear}} - \mathbf{g} \tag{2.1}$$

where $\mathbf{a}_{\text{linear}}$ is the linear acceleration of the sensor and $\mathbf{g}$ is the gravitational acceleration vector. All vectors in this equation are expressed in the same coordinate frame. When the sensor is stationary, $\mathbf{a}_{\text{linear}} \approx 0$, and the measured output directly reflects the direction of gravity. This allows the accelerometer to estimate the inclination of the sensor relative to the vertical:

$$\theta_{\text{acc}} = \arctan\left(\frac{a_y}{a_z}\right) \tag{2.2}$$

where a_y and a_z are two orthogonal accelerometer components in the sensor coordinate frame. However, during dynamic motion, linear accelerations corrupt the inclination estimate [28].

2.1.2 Gyroscope

A gyroscope measures angular velocity $\boldsymbol{\omega}$ about the sensor axes. The orientation change over time can be estimated by integrating the angular velocity:

$$\boldsymbol{\theta}(t) = \boldsymbol{\theta}(t_0) + \int_{t_0}^{t} \boldsymbol{\omega}(\tau)\, d\tau \tag{2.3}$$

Gyroscopes provide accurate short-term orientation tracking and are not affected by linear accelerations. However, integration of noise over time leads to a gradual accumulation of error known as gyroscope drift. This makes the orientation estimate to diverge from the true value over time [29].

2.1.3 Magnetometer

A magnetometer measures the local magnetic field vector, which provides a reference for heading estimation relative to magnetic north. It can correct for gyroscope drift in the heading direction. However, magnetometer measurements are sensitive to disturbances from nearby ferromagnetic materials or electrical equipment [29]. In this thesis, the magnetometer was disabled due to magnetic disturbances in the experimental environment, and a sensor fusion approach using only the accelerometer and gyroscope was used instead.

2.2 Sensor Fusion and the Kalman Filter

Each individual sensor has limitations: the accelerometer is corrupted by dynamic accelerations, the gyroscope suffers from drift, and the magnetometer is sensitive to magnetic disturbances. Sensor fusion algorithms combine the complementary strengths of multiple sensors to produce a more accurate and stable orientation estimate [30].
Several sensor fusion algorithms have been proposed for IMU-based orientation estimation.
The complementary filter splits sensor signals by frequency, using high-frequency gyroscope data for short-term tracking and low-frequency accelerometer data to correct drift [30]. This approach is computationally simple and easy to implement, making it suitable for real-time applications on low-power hardware. However, it relies on a fixed tuning parameter to balance the two sensor sources, which may not perform consistently across different motion conditions [30].
The Madgwick filter uses a gradient descent optimisation approach to fuse accelerometer, gyroscope, and optionally magnetometer data [31]. It is computationally efficient and suitable for real-time implementation. The filter includes a single gain parameter that controls the correction rate, making parameter tuning relatively straightforward. However, it assumes that accelerometer measurements primarily reflect gravity, and its performance may degrade during highly dynamic movements where linear accelerations are significant [31].
The extended Kalman filter (EKF) provides an optimal recursive estimator under Gaussian noise assumptions [32]. It explicitly models the noise characteristics of each sensor and dynamically adjusts the weighting between sensors according to the estimated uncertainty. Compared with simpler filters, the EKF generally provides greater robustness under varying motion conditions. [32].

The Movella DOT sensors used in this thesis employ an EKF-based algorithm called XKFCore embedded in the device firmware. The algorithm operates internally at 800 Hz and outputs orientation data at 60 Hz.
The EKF operates as a recursive estimator that maintains an estimate of the system state and updates it as new sensor measurements arrive. The filter consists of two steps: prediction and update.
The following equations describe the general prediction and update steps of a discrete Kalman filter [33].
Prediction step: The orientation state $\hat{\mathbf{x}}$ is predicted forward in time using the gyroscope measurements:

$$\hat{\mathbf{x}}_{k|k-1} = \mathbf{F}_k \hat{\mathbf{x}}_{k-1|k-1} \tag{2.4}$$

$$\mathbf{P}_{k|k-1} = \mathbf{F}_k \mathbf{P}_{k-1|k-1} \mathbf{F}_k^\top + \mathbf{Q}_k \tag{2.5}$$

where $\mathbf{F}_k$ is the state transition matrix derived from the gyroscope angular velocity, $\mathbf{P}$ is the state covariance matrix, and $\mathbf{Q}_k$ is the process noise covariance representing gyroscope noise and drift.
Update step: The predicted state is corrected using the accelerometer measurements:

$$\mathbf{K}_k = \mathbf{P}_{k|k-1} \mathbf{H}_k^\top \left(\mathbf{H}_k \mathbf{P}_{k|k-1} \mathbf{H}_k^\top + \mathbf{R}_k \right)^{-1} \tag{2.6}$$

$$\hat{\mathbf{x}}_{k|k} = \hat{\mathbf{x}}_{k|k-1} + \mathbf{K}_k \left(\mathbf{z}_k - \mathbf{H}_k \hat{\mathbf{x}}_{k|k-1} \right) \tag{2.7}$$

$$\mathbf{P}_{k|k} = \left(\mathbf{I} - \mathbf{K}_k \mathbf{H}_k \right) \mathbf{P}_{k|k-1} \tag{2.8}$$

where $\mathbf{K}_k$ is the Kalman gain, $\mathbf{z}_k$ is the measurement vector from the accelerometer, $\mathbf{H}_k$ is the measurement matrix, and $\mathbf{R}_k$ is the measurement noise covariance.
The Kalman gain $\mathbf{K}_k$ determines how much weight is given to the new measurement versus the prediction. In general, when the sensor is stationary, the filter relies more on the accelerometer to correct gyroscope drift. When the sensor is moving rapidly, the filter relies more on the gyroscope prediction. In this way, the filter continuously balances the strengths of each sensor to produce a stable orientation estimate [32].

2.3 Orientation Representation

The orientation of a body segment estimated by an IMU can be represented in different mathematical forms. Two common representations are Euler angles and quaternions.

2.3.1 Euler Angles

Euler angles describe orientation as three successive rotations about defined axes, typically reported as roll (ϕ), pitch (θ), and yaw (ψ) [34]:

$$\mathbf{R} = \mathbf{R}_z(\psi)\,\mathbf{R}_y(\theta)\,\mathbf{R}_x(\phi) \tag{2.9}$$

where $\mathbf{R}_x$, $\mathbf{R}_y$, $\mathbf{R}_z$ are elementary rotation matrices about each axis. Euler angles are intuitive and easy to interpret clinically, as they correspond to anatomically meaningful rotation axes such as flexion–extension and lateral bending. However,

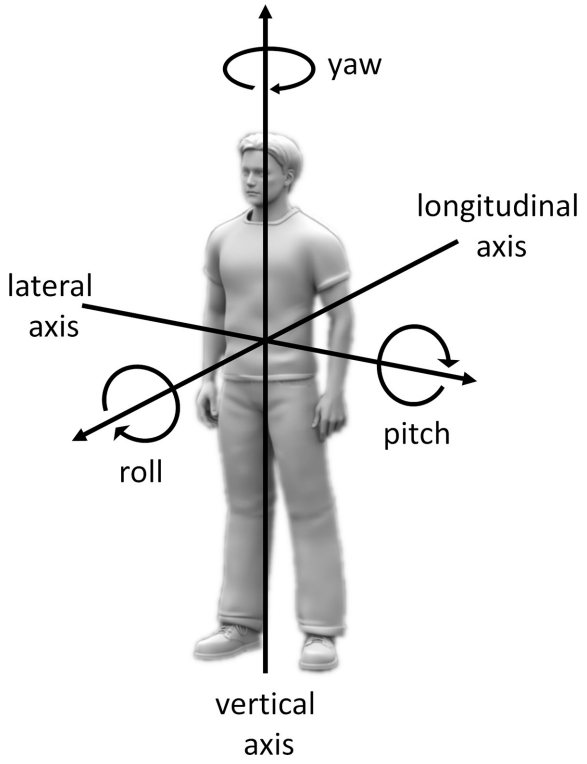

Figure 2.1: Illustration of roll, pitch, and yaw rotations. Adapted from [35].

Euler angles suffer from a singularity condition known as gimbal lock, which occurs when two rotation axes become aligned, causing a loss of one degree of freedom and numerical instability [34]. This is most likely to occur during large or multi-planar movements.

2.3.2 Quaternions

A unit quaternion represents orientation using a four-component vector:

$$\mathbf{q} = w + x\mathbf{i} + y\mathbf{j} + z\mathbf{k}, \quad \text{with } w^2 + x^2 + y^2 + z^2 = 1 \tag{2.10}$$

where w is the scalar part and x, y, z form the vector part. A quaternion can also be written in terms of a rotation axis $\hat{\mathbf{n}}$ and rotation angle α:

$$\mathbf{q} = \cos\frac{\alpha}{2} + \sin\frac{\alpha}{2}(n_x\mathbf{i} + n_y\mathbf{j} + n_z\mathbf{k}) \tag{2.11}$$

Quaternions are free from gimbal lock singularities and provide numerically stable orientation tracking [36]. Sensor fusion algorithms such as the EKF and Madgwick filter natively operate in quaternion space [31].

A quaternion can be converted to a 3×3 rotation matrix using the standard quaternion-to-rotation-matrix relationship [37]:

$$\mathbf{R} = \begin{pmatrix} 1-2(y^2+z^2) & 2(xy-wz) & 2(xz+wy) \\ 2(xy+wz) & 1-2(x^2+z^2) & 2(yz-wx) \\ 2(xz-wy) & 2(yz+wx) & 1-2(x^2+y^2) \end{pmatrix} \tag{2.12}$$

This rotation matrix describes the orientation of the sensor frame relative to the global frame.

3
Methods

This chapter describes the experimental methods used in this thesis. It is divided into two parts. Part A investigates the accuracy and reliability of IMU-based sagittal posture estimation across multiple body segments, using a Qualisys MoCap system as the ground truth. Part B investigates the feasibility of IMU-based respiration monitoring using relative thoracic orientation.
The two parts are closely related. Breathing produces rhythmic thoracic motion that introduces low-frequency oscillations into IMU-derived orientation signals [38], particularly for sensors placed on the thorax. This raises two questions: first, how does breathing affect the accuracy of thorax-mounted IMU posture measurements; and second, can this breathing-induced thoracic motion be exploited as a respiration monitoring signal. Part A addresses the first question, and Part B addresses the second.

3.1 Part A: IMU-Based Sagittal Posture Estimation

3.1.1 Participants

Four healthy adults participated in this study (two males and two females). All participants completed repeated posture measurement trials under different experimental conditions. The experiments focused on sagittal-plane posture assessment during static standing and controlled posture tasks. Before data collection, all participants were informed about the experimental procedures.

3.1.2 Experimental Setup

The experiments were conducted using Movella DOT inertial measurement units (IMUs) and a Qualisys optical motion capture (MoCap) system as the reference.
The Movella DOT IMUs integrate a triaxial accelerometer, gyroscope, and magnetometer. However, only the accelerometer and gyroscope data were used in this study, to avoid magnetic disturbances in the experimental environment. Orientation estimates were computed using a six-axis Kalman-filter–based sensor fusion algorithm embedded in the device. IMU data were collected using the Movella DOT mobile application and exported in quaternion format at a sampling rate of 60 Hz for post-processing.

A Qualisys optical motion capture system was used as the reference measurement system for posture validation. The MoCap system provided reference segment orientations for comparison with the IMU-based estimates. Both systems operated at a sampling rate of 60 Hz.
Temporal synchronisation between the IMU and MoCap systems was achieved during post-processing using a cross-correlation–based alignment procedure.

3.1.3 Sensor Placement and Calibration

IMUs were attached to the body using elastic fixation straps to minimise sensor movement relative to the skin surface. Sensors were positioned at the following anatomical locations:

- Sacral region (approximately S1) for pelvic motion measurement
- Mid-sternum region for thorax motion measurement
- C7/T1 region for cervical posture measurement
- Forehead (frontal region) for head posture measurement
- Upper back region for thoracic respiratory motion measurement

For MoCap-based reference measurements, pairs of retroreflective markers were placed directly above and below each IMU attachment site, along the longitudinal axis of the corresponding body segment. This arrangement ensured that both the IMU and MoCap markers were subject to the same soft-tissue motion during measurement. Segment longitudinal vectors were computed as the vector from the inferior to the superior marker, pointing upward along the segment axis.
Figure 3.1 shows the sensor and marker placement used in this study.

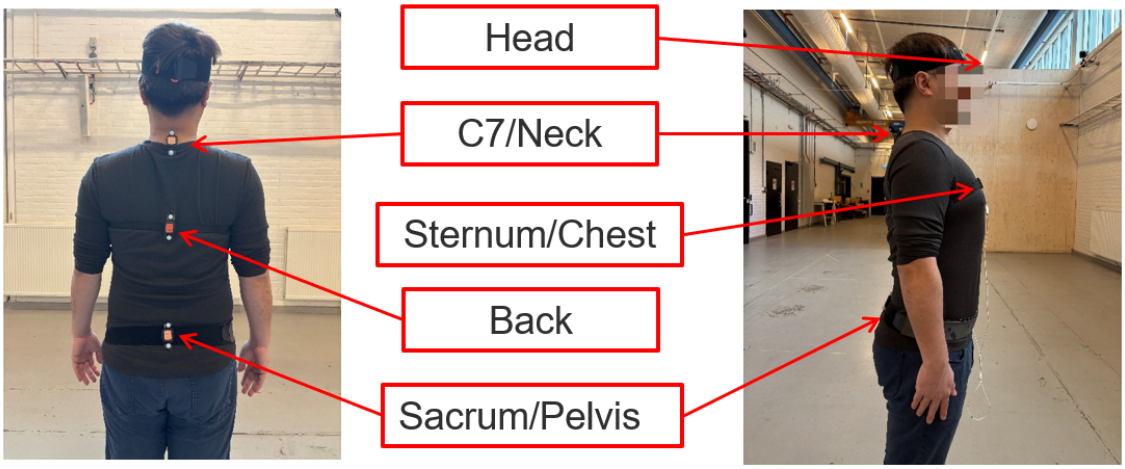

Figure 3.1: Sensor and marker placement on the participant.

Before each recording session, participants performed a static neutral standing calibration. During calibration, participants stood upright with arms relaxed at the sides and gaze directed forward. The mean sensor orientation during the first five seconds of the static calibration interval was used as the neutral reference posture for subsequent angle calculations.

3.1.4 Orientation Estimation

Figure 3.2: Local coordinate system of the Xsens IMU sensor.

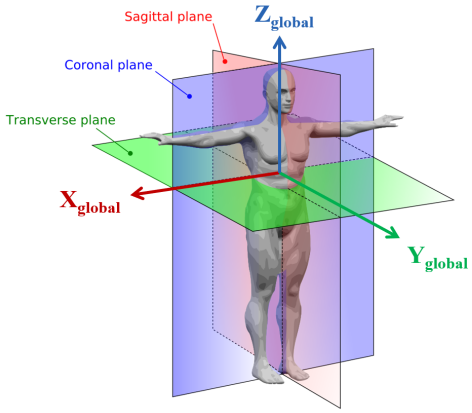

Figure 3.3: Anatomical planes of the human body.

Each sensor was mounted with its x-axis pointing upward along the body segment, the z-axis pointing in the anterior–posterior direction, and the y-axis pointing laterally (Figure 3.2). The global frame was defined with Z_{global} pointing vertically upward, X_{global} pointing anteriorly, and Y_{global} pointing to the right (Figure 3.3), such that the sensor x-axis aligned with the global vertical direction during neutral standing.

3.1.4.1 Quaternion-Based Tilt Computation

The sagittal tilt angle θ was defined as the angle between the sensor x-axis and the global vertical axis Z_{global} (Figure 3.4). The orientation of the sensor x-axis in the global frame was first obtained from the quaternion-derived rotation matrix. Here, $\mathbf{R}(t)$ was computed from the sensor quaternion at time t using the quaternion-to-rotation-matrix relationship described in Equation 2.12:

$$\mathbf{x}_{\text{global}}(t) = \mathbf{R}(t)\,\hat{\mathbf{e}}_x \tag{3.1}$$

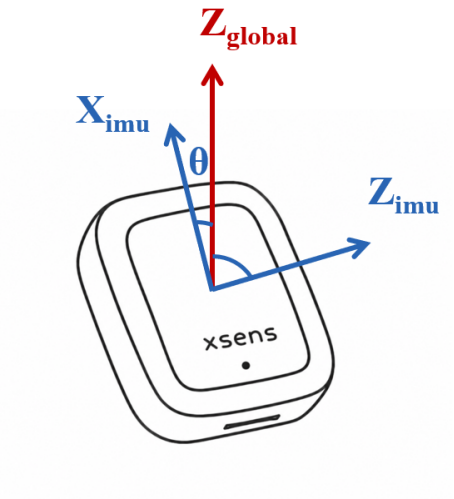

Figure 3.4: Quaternion-based sagittal tilt definition

where $\hat{\mathbf{e}}_x = [1, 0, 0]^\top$ is the unit vector of the sensor x-axis. The sagittal tilt angle was then computed from the anterior–posterior component of $\mathbf{x}_{\text{global}}$:

$$\theta^{\text{IMU}}(t) = \arcsin\left(x_{\text{ant}}(t)\right) \cdot s \tag{3.2}$$

where $x_{\text{ant}}(t)$ denotes the component of $\mathbf{x}_{\text{global}}(t)$ along the anterior–posterior global axis. In the coordinate system used in this thesis, this corresponds to the X_{global} component. The factor $s \in \{-1, +1\}$ is a sign correction factor used to compensate for the reversed mounting orientation between anteriorly and posteriorly mounted sensors.

3.1.4.2 Euler-Angle-Based Tilt Estimation

Sagittal tilt was estimated using the Euler-angle output (X, Y, Z) recorded directly from the Movella DOT app. In this thesis, $Y(t)$ and $Z(t)$ denote the Y- and Z-components of the Euler-angle output at time t, expressed in degrees.
This Euler-angle-based method was based on the observed output characteristics of the Movella DOT app under the sensor mounting configuration used in this study. When the sensor was mounted upright, with its local x-axis aligned approximately with the vertical body-segment direction, the app-reported Y-component was approximately $-90°$. When the sensor was tilted forward or backward towards a more horizontal orientation, the absolute value of the Y-component decreased towards $0°$. Therefore, the term $90° - |Y(t)|$ was used to represent the magnitude of sagittal tilt away from the upright orientation.
The sign of the Z-component was used to determine the direction of tilt. In the evaluated posture range, positive and negative values of $Z(t)$ corresponded to opposite sagittal tilt directions. A sensor-specific sign correction factor was then applied to account for differences in mounting orientation between anteriorly and posteriorly placed sensors.
Figure 3.5 illustrates the sagittal tilt angle definition used in this thesis. The angle θ shown in the figure represents the sagittal tilt angle estimated from the Euler-angle

output, not the Y-component itself.

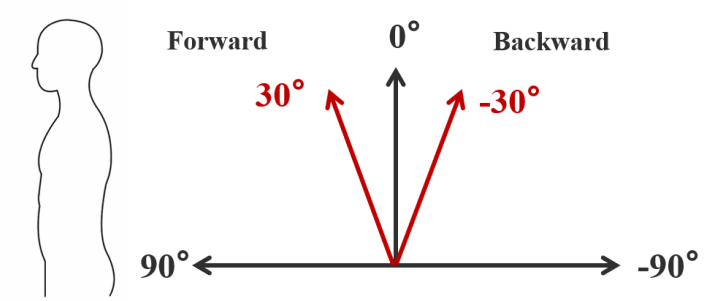

Figure 3.5: Schematic diagram of sagittal tilt angle definition. The angle θ represents the sagittal tilt angle relative to the upright orientation.

Based on this empirical relationship, the Euler-angle-based sagittal tilt was computed as:

$$\theta_{\text{Euler}}(t) = (90^\circ - |Y(t)|) \cdot \text{sign}(Z(t)) \cdot s \tag{3.3}$$

where $Y(t)$ and $Z(t)$ are the Y- and Z-components of the Euler-angle output from the Movella DOT app at time t, and $s \in \{-1, +1\}$ is a sensor-specific sign correction factor used to compensate for reversed sensor mounting orientations.

3.1.5 Posture Variables

Prior to comparative analysis, all signals were zeroed by subtracting the mean value of a static standing period at the beginning of each trial. This step was applied to remove the systematic offset between the MoCap and IMU systems, so that the two signals could be compared on the same baseline.

3.1.5.1 Pelvic Tilt

Pelvic tilt was defined as the absolute sagittal-plane orientation of the pelvic segment. Positive values represented anterior pelvic tilt, while negative values represented posterior pelvic tilt. For MoCap-based estimation, pelvic tilt was computed as:

$$\theta_P(t) = \text{atan2}(v_{P,y}(t),\, v_{P,z}(t))$$

where $v_{P,y}$ and $v_{P,z}$ denote the anterior–posterior and vertical components of the pelvic longitudinal vector, respectively.

3.1.5.2 Thorax Tilt

Thorax tilt was defined as the absolute sagittal-plane orientation of the thoracic segment. Positive values represented forward thoracic inclination. For MoCap-based estimation, thorax tilt was computed as:

$$\theta_T(t) = \text{atan2}(v_{T,y}(t),\, v_{T,z}(t))$$

where $v_{T,y}$ and $v_{T,z}$ denote the anterior–posterior and vertical components of the thoracic longitudinal vector, respectively.

3.1.5.3 Thorax–Pelvis Relative Alignment

Thorax–pelvis relative alignment was calculated as the angular difference between thorax tilt and pelvic tilt:

$$\theta_{TP}(t) = \theta_T(t) - \theta_P(t)$$

where $\theta_T(t)$ represents thorax tilt and $\theta_P(t)$ represents pelvic tilt at time t.

3.1.5.4 Forward Head Posture (FHP)

Forward head posture (FHP) was quantified as the relative sagittal orientation between the head segment and the cervical segment (C7):

$$\theta_{\mathrm{FHP}}(t) = \theta_H(t) - \theta_{C7}(t)$$

where $\theta_H(t)$ represents head tilt and $\theta_{C7}(t)$ represents cervical segment tilt at time t.

3.1.6 Experimental Protocol

3.1.6.1 Static Posture Tasks

Each participant performed a series of controlled sagittal-plane posture tasks during standing. The following posture conditions were included:

- Neutral standing
- Anterior pelvic tilt
- Posterior pelvic tilt
- Forward thorax inclination
- Backward thorax inclination
- Forward head posture (FHP)

A schematic illustration of the posture tasks is shown in Figure 3.6.
The posture tasks were divided into three trials for each participant. Each trial was recorded as one continuous data segment. The thorax trial included two repetitions of forward thorax inclination followed by two repetitions of backward thorax inclination. The pelvis trial included two repetitions of anterior pelvic tilt followed by two repetitions of posterior pelvic tilt. The FHP trial included two repetitions of forward head posture.

3.1.6.2 Breathing Conditions

To investigate the influence of respiratory motion on thorax-related posture estimation, an additional breathing trial was conducted during the forward thorax inclination task. This posture was selected because respiratory motion was expected to mainly affect thorax-mounted IMU measurements.

(a) Neutral standing

(b) Anterior pelvic tilt

(c) Posterior pelvic tilt

(d) Forward thorax inclination

(e) Backward thorax inclination

(f) Forward head posture (FHP)

Figure 3.6: Six posture conditions evaluated in this study.

During this trial, participants were instructed to perform deep breathing while maintaining a forward thorax inclination posture. All four participants completed one additional breathing trial. For each participant, this trial consisted of two repetitions of forward thorax inclination with deep breathing, recorded as one continuous segment. These data were used to evaluate whether respiratory motion introduced additional variability or oscillatory disturbances into the thorax tilt estimates.

3.1.7 Data Processing

All IMU and MoCap signals were processed offline using MATLAB (MathWorks, Natick, MA, USA). The processing pipeline included temporal synchronisation, gap filling, filtering, signal interpolation, and quantitative comparison between IMU-based estimates and MoCap reference signals.

3.1.7.1 Temporal Synchronisation

Since the IMU and MoCap systems were not hardware-triggered, temporal synchronisation was achieved in post-processing using a cross-correlation–based alignment procedure. Both signals were first interpolated onto a common time base derived

from the MoCap sampling interval. Mean subtraction was applied prior to cross-correlation to remove DC offsets. The normalised cross-correlation between the IMU and MoCap reference signals was computed over a maximum lag window of five seconds, and the lag corresponding to the peak correlation coefficient was identified. The optimal time shift was then applied to the full IMU time axis before subsequent comparison.

3.1.7.2 Gap Filling and Filtering

Short gaps in MoCap marker trajectories (up to 10 consecutive frames) were filled using linear interpolation prior to filtering. MoCap posture signals were filtered using a fourth-order zero-phase Butterworth low-pass filter with a cutoff frequency of 3 Hz. IMU quaternion-derived tilt signals were smoothed using a Savitzky–Golay filter (polynomial order 3, frame length 11 samples). Both filters were applied to attenuate high-frequency noise and soft-tissue motion artefacts.

3.1.7.3 Signal Alignment and Interpolation

Following temporal synchronisation, IMU signals were interpolated onto the MoCap time axis using linear interpolation to enable sample-by-sample comparison. Only time points with valid (non-NaN) samples in both signals were included in the quantitative evaluation.

3.1.8 Evaluation Metrics

The performance of the IMU-based posture estimation system was evaluated in terms of accuracy and repeatability using the following quantitative metrics.

3.1.8.1 Root Mean Square Error (RMSE)

Root Mean Square Error (RMSE) was used to quantify the magnitude of the difference between IMU-based posture estimates and the MoCap reference:

$$\mathrm{RMSE} = \sqrt{\frac{1}{N}\sum_{k=1}^{N}\left(\theta^{\mathrm{IMU}}(k) - \theta^{\mathrm{MoCap}}(k)\right)^2}$$

where N denotes the total number of valid samples.

3.1.8.2 Coefficient of Determination (R^2)

The coefficient of determination (R^2) was computed as the squared Pearson correlation coefficient between the IMU and MoCap signals:

$$R^2 = \left(\frac{\sum_{k=1}^{N}\left(\theta^{\mathrm{IMU}}(k) - \overline{\theta^{\mathrm{IMU}}}\right)\left(\theta^{\mathrm{MoCap}}(k) - \overline{\theta^{\mathrm{MoCap}}}\right)}{\sqrt{\sum_{k=1}^{N}\left(\theta^{\mathrm{IMU}}(k) - \overline{\theta^{\mathrm{IMU}}}\right)^2 \sum_{k=1}^{N}\left(\theta^{\mathrm{MoCap}}(k) - \overline{\theta^{\mathrm{MoCap}}}\right)^2}} \right)^2$$

Higher R^2 values indicate stronger linear agreement between the two measurement systems.

3.1.8.3 Intraclass Correlation Coefficient (ICC)

Intraclass correlation coefficient (ICC(3,1): two-way mixed effects, consistency, single measurement) was used to evaluate measurement repeatability across repeated trials [39]. The ICC was computed as:

$$\mathrm{ICC}(3,1) = \frac{MS_R - MS_E}{MS_R + (k-1)\,MS_E}$$

where MS_R is the mean square for rows, representing variability between the evaluated samples, MS_E is the residual mean square error, and k is the number of measurement methods. In this study, $k = 2$, corresponding to the IMU-based estimate and the MoCap reference. The mean square terms were obtained from the two-way ANOVA table used for the ICC(3,1) calculation. ICC values below 0.50 were considered poor, values between 0.50 and 0.75 moderate, values between 0.75 and 0.90 good, and values above 0.90 excellent [39].

3.2 Part B: IMU-Based Respiration Monitoring

3.2.1 Participants

Three participants from Part A (one male and two females) took part in the respiration monitoring experiment.

3.2.2 Experimental Setup

The experiment was conducted using two Movella DOT IMUs and a BioSignalsPlux respiratory belt (Plux Wireless Biosignals) as the reference. IMU data were recorded at 60 Hz using the Movella DOT mobile application and exported in quaternion format for post-processing. The belt signal was sampled at 20 Hz and exported via the OpenSignals software platform. Participants performed the experiment in both standing and sitting positions, under two breathing conditions: normal breathing and deep breathing. Each condition was repeated twice per participant per position.

3.2.3 Sensor Placement

Two Movella DOT IMUs were positioned on the anterior (chest) and posterior (back) thoracic surface at the same height, aligned horizontally at mid-thorax level.Both IMUs were attached directly onto the BioSignalsPlux respiratory belt, which was secured around the participant's thorax. This placement ensured that the IMUs and the respiratory belt moved together during breathing.

(a) Front view **(b)** Side view **(c)** Back view

Figure 3.7: Sensor placement for respiratory monitoring. Two Movella DOT IMUs were attached to the anterior and posterior thoracic surface, aligned with the BioSignalsPlux respiratory belt.

3.2.4 Reference Respiratory Signal

The BioSignalsPlux respiratory belt was used as the reference measurement for respiratory monitoring validation. The belt records thoracic circumference changes associated with breathing effort. Prior to analysis, the belt signal was baseline-corrected by mean subtraction and linear detrending, then filtered using a second-order zero-phase Butterworth bandpass filter with a passband of 0.1–0.6 Hz to isolate the respiratory frequency range. Additional smoothing was applied using a Savitzky–Golay filter (polynomial order 3, frame length 11 samples).

3.2.5 IMU-Based Respiratory Signal Extraction

The IMU-based respiratory signal was derived from the relative orientation between the chest and back IMUs. For each IMU, quaternion data were recorded at 60 Hz and preprocessed using quaternion normalisation and continuity enforcement. A quaternion sign correction (`quatFlipZ`) was applied to the back sensor to align its coordinate frame with that of the chest sensor.
The relative orientation between the two sensors was computed in quaternion space as:

$$\mathbf{q}_{\text{rel}}(t) = \mathbf{q}_{\text{back}}^{-1}(t) \otimes \mathbf{q}_{\text{chest}}(t)$$

where $\mathbf{q}_{\text{back}}^{-1}$ denotes the quaternion conjugate of the back sensor orientation. This relative quaternion represents the chest rotation relative to the back. It captures thoracic expansion during breathing while reducing movement artefacts common to both sensors.
The relative quaternion was converted to Euler angles using an XYZ rotation sequence. Based on the sensor mounting orientation (local x-axis aligned with the

body longitudinal axis, y-axis lateral, z-axis anterior–posterior), rotation about the y-axis was identified as the primary breathing axis, corresponding to anterior–posterior thoracic expansion. The respiratory signal was therefore extracted as the y-axis Euler angle component of $\mathbf{q}_{\text{rel}}$.
The extracted signal was then processed with a second-order zero-phase Butterworth bandpass filter (0.1–0.6 Hz) to isolate the respiratory frequency component, followed by zero-point correction using a reference window of 5–10 s from the beginning of each trial.

3.2.6 Comparison and Evaluation

Both the IMU-derived and belt-reference respiratory signals were normalised to zero mean and unit standard deviation prior to comparison. Temporal alignment between the IMU-derived and belt-reference respiratory signals was achieved using a cross-correlation–based procedure, consistent with the synchronisation method described in Section 3.1.7.
The two signals were resampled to a common time axis at 20 Hz using linear interpolation. The following metrics were used to evaluate the agreement between the IMU-based and reference respiratory signals:

- **Pearson correlation coefficient** (r): to quantify the linear relationship between the normalised IMU and belt waveforms.
- **Root mean square error (RMSE)**: to quantify the magnitude of waveform differences after normalisation.

4

Results

This chapter presents the results of both parts of the study. Part A reports the accuracy and reliability of IMU-based sagittal posture estimation, the comparison between Euler-angle and quaternion methods, and the influence of deep breathing on thorax tilt estimation. Part B presents the agreement between IMU-derived and belt-reference respiratory signals under different breathing and body positions.

4.1 Part A: IMU-Based Sagittal Posture Estimation

4.1.1 Posture Estimation Accuracy

Table 4.1 summarises the accuracy and reliability metrics for each sagittal posture variable. The metrics were averaged across four participants. Results are reported as mean ± standard deviation.

Table 4.1: Accuracy and reliability of IMU-based sagittal posture estimation compared with the MoCap reference system.

Variable	RMSE (deg)	R^2	ICC
Pelvic tilt	0.864 ± 0.271	0.996 ± 0.004	0.997 ± 0.003
Thorax tilt	1.651 ± 0.553	0.974 ± 0.045	0.985 ± 0.024
Thorax–pelvis alignment	1.815 ± 0.565	0.971 ± 0.032	0.968 ± 0.038
FHP	2.012 ± 1.446	0.749 ± 0.281	0.799 ± 0.185

Figure 4.1 shows a representative time-series comparison between IMU-based and MoCap-based posture estimates for one participant, including pelvic tilt, thorax tilt, and thorax–pelvis alignment. Time-series plots for all participants are provided in Appendix A.1.
Overall, pelvic tilt demonstrated the lowest RMSE ($0.864 \pm 0.271°$), while FHP showed the highest RMSE ($2.012 \pm 1.446°$). ICC values indicated excellent repeatability for pelvic tilt, thorax tilt, and thorax–pelvis alignment (ICC > 0.96), and good repeatability for FHP (ICC $= 0.799 \pm 0.185$).

4.1.2 Comparison of Euler-Angle and Quaternion Methods

Figure 4.2 shows the overlay of Euler-angle–based and quaternion-based sagittal tilt estimates for thorax anterior tilt, thorax posterior tilt, and pelvic tilt. In all cases,

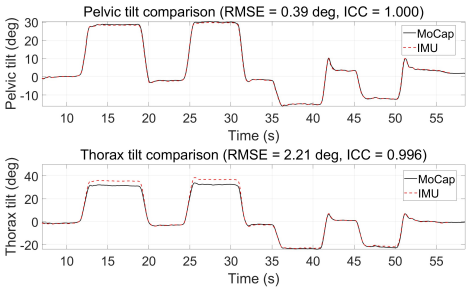

(a) Thorax forward and backward tilt

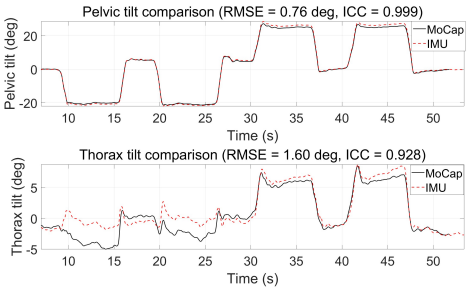

(b) Pelvic posterior and anterior tilt

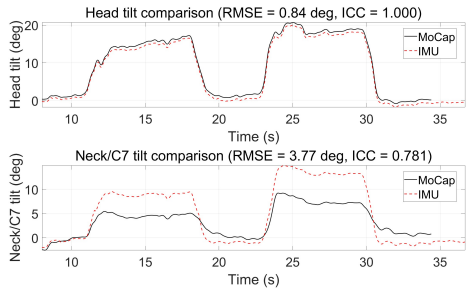

(c) Head tilt and neck tilt

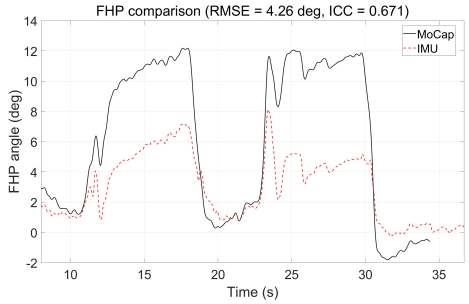

(d) Forward head posture (FHP)

Figure 4.1: Representative time-series comparison between IMU (dashed red) and MoCap (solid black) posture estimates for participant S01.

the two curves were visually indistinguishable throughout the majority of each trial. Table 4.2 summarises the quantitative differences between the two orientation representation methods across the three evaluated posture tasks.

Table 4.2: Quantitative differences between Euler-angle-based and quaternion-based sagittal tilt estimates.

Posture Task	Mean Abs. Diff. (deg)	Max Abs. Diff. (deg)
Thorax anterior tilt	0.40	2.92
Thorax posterior tilt	0.07	2.09
Pelvic tilt	0.46	4.95

Mean absolute differences between the two methods were below 0.5° for all evaluated conditions. The smallest difference was observed during thorax posterior tilt (mean 0.07°), while pelvic tilt showed the largest maximum instantaneous difference (4.95°). These peak differences were transient and occurred primarily during motion transitions rather than during sustained posture holds.

Overall, the results indicate that Euler-angle–based and quaternion-based orientation representations produced highly comparable sagittal tilt estimates under the experimental conditions evaluated. The negligible mean differences suggest that either method is suitable for quasi-static sagittal posture assessment within the angular ranges tested.

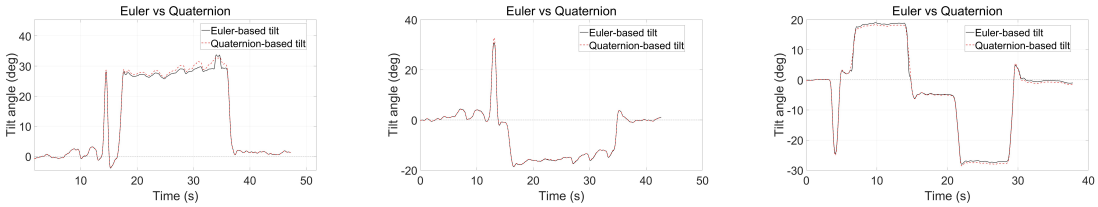

(a) Thorax anterior tilt **(b)** Thorax posterior tilt **(c)** Pelvic tilt

Figure 4.2: Overlay of Euler-angle–based (solid black) and quaternion-based (dashed red) sagittal tilt estimates for three body positions. The two curves show close agreement throughout all trials.

4.1.3 Influence of Deep Breathing on Thorax Tilt Estimation

The influence of deep breathing on thorax tilt estimation was investigated by visual inspection of IMU and MoCap signal comparisons during deep breathing trials. Figure 4.3 shows the thorax tilt comparisons for all four participants during deep breathing while maintaining a forward thorax inclination posture.

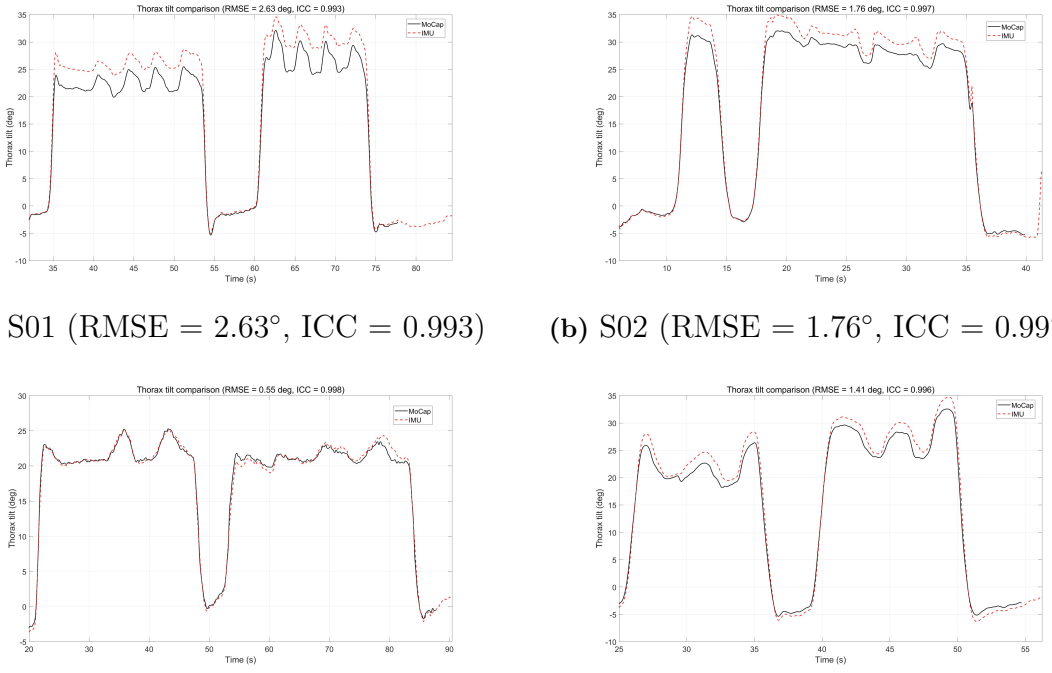

(a) S01 (RMSE = 2.63°, ICC = 0.993) **(b)** S02 (RMSE = 1.76°, ICC = 0.997)

(c) S03 (RMSE = 0.55°, ICC = 0.998) **(d)** S04 (RMSE = 1.41°, ICC = 0.996)

Figure 4.3: Thorax tilt comparison between IMU (dashed red) and MoCap (solid black) for all four participants during deep breathing.

Across all four participants, periodic oscillations were clearly visible in both IMU and MoCap thorax tilt signals during deep breathing. These oscillations reflect the rhythmic thoracic expansion associated with respiratory motion. ICC values remained high across all participants (range: 0.993–0.998), indicating that overall

motion tracking agreement was well maintained during deep breathing. However, RMSE values showed considerable inter-subject variability, ranging from 0.55° (S03) to 2.63° (S01).
In participants with higher RMSE values (S01, S02), an apparent offset of the IMU estimate relative to the MoCap reference was observed during the forward inclination posture. This offset may reflect differences in how the two systems respond to soft-tissue deformation caused by thoracic expansion. In contrast, S03 showed close IMU–MoCap agreement with minimal offset.
It should be noted that MoCap markers were positioned directly on the IMU attachment straps. Therefore, both systems were subject to the same respiratory soft-tissue displacement. The reported RMSE values reflect differences between the IMU-based estimates and the MoCap marker-based reference, rather than the absolute measurement error of the IMU system relative to true skeletal motion.

4.2 Part B: IMU-Based Respiration Monitoring

Tables 4.3 and 4.4 summarise the agreement between IMU-derived respiratory signals and the BioSignalsPlux belt reference for three participants under standing and sitting conditions, respectively.

Table 4.3: Agreement between IMU-derived and belt-reference respiratory signals during standing across three participants.

	Normal Breathing		**Deep Breathing**	
Subject	**Pearson r**	**RMSE**	**Pearson r**	**RMSE**
S01	0.579	0.927	0.964	0.308
S02	0.582	0.921	0.923	0.424
S03	0.412	1.110	0.803	0.650

Table 4.4: Agreement between IMU-derived and belt-reference respiratory signals during sitting across three participants.

	Normal Breathing		**Deep Breathing**	
Subject	**Pearson r**	**RMSE**	**Pearson r**	**RMSE**
S01	0.700	0.757	0.960	0.310
S02	0.725	0.755	0.952	0.337
S03	0.406	1.113	0.881	0.496

Across both body positions, deep breathing consistently yielded higher agreement compared with normal breathing. During deep breathing, Pearson r values ranged from 0.803 to 0.964 (standing) and from 0.881 to 0.960 (sitting). During normal breathing, agreement was lower and more variable, with Pearson r ranging from 0.412 to 0.582 (standing) and from 0.406 to 0.725 (sitting). The difference between standing and sitting was small for most participants. S01 and S02 showed consistently higher agreement with the belt reference compared with S03, particularly

during normal breathing, where S03 showed Pearson r of 0.412 (standing) and 0.406 (sitting) compared with values above 0.57 for S01 and S02.
Figure 4.4 shows the normalised IMU-derived and belt-reference respiratory signals for participant S01 under all four conditions.

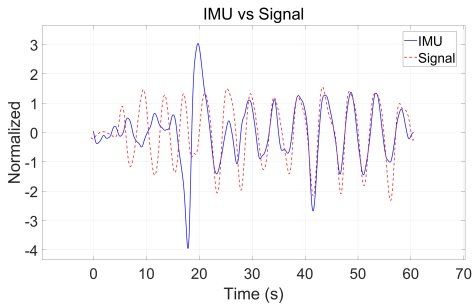

(a) Sitting, normal breathing ($r = 0.700$, RMSE = 0.757)

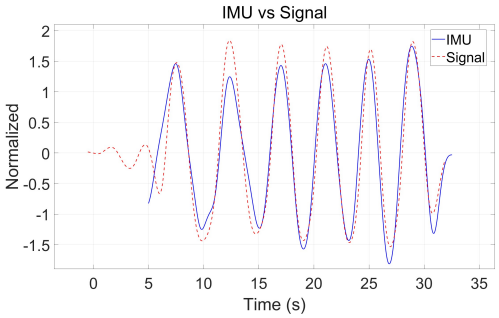

(b) Sitting, deep breathing ($r = 0.960$, RMSE = 0.310)

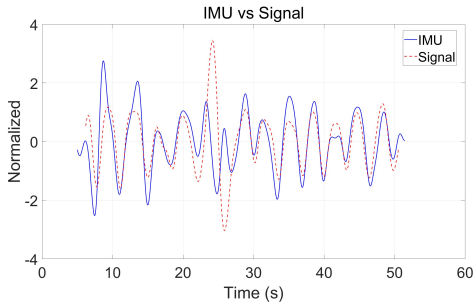

(c) Standing, normal breathing ($r = 0.579$, RMSE = 0.927)

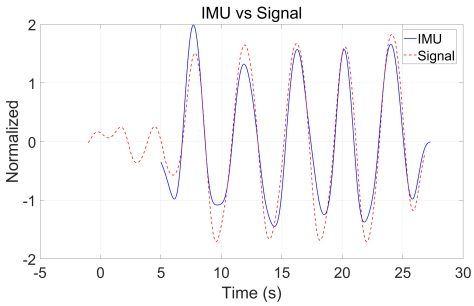

(d) Standing, deep breathing ($r = 0.964$, RMSE = 0.308)

Figure 4.4: Comparison between normalised IMU-derived respiratory signal (blue) and BioSignalsPlux belt reference (dashed red) for participant S01 under four conditions.

5

Discussion

This chapter interprets the findings of the study in relation to the research questions and discusses their implications. Part A covers the accuracy and reliability of IMU-based sagittal posture estimation, the comparison between orientation representation methods, and the influence of breathing on thorax-mounted IMU measurements. Part B discusses the feasibility of IMU-based respiration monitoring. General limitations of the study are addressed at the end of the chapter.

5.1 Part A: IMU-Based Sagittal Posture Estimation

5.1.1 IMU-Based Sagittal Posture Estimation Accuracy

The results demonstrated that IMU-based sagittal posture estimation achieved good to excellent agreement with the MoCap reference across most measurement variables. Pelvic tilt showed the highest accuracy, with a mean RMSE of 0.864° and ICC of 0.997, followed by thorax tilt (RMSE = 1.651°, ICC = 0.985) and thorax–pelvis alignment (RMSE = 1.815°, ICC = 0.968).

The superior accuracy of pelvic tilt estimation is consistent with the anatomical characteristics of the sacral region. The sacrum has less soft tissue compared with the thorax, which may reduce movement artefacts in IMU measurements. In contrast, the thorax is surrounded by a larger volume of soft tissue and musculature, and is subject to respiratory motion, both of which may contribute to greater measurement variability.

The thorax–pelvis alignment showed slightly higher RMSE compared with thorax tilt alone, which is expected given that this variable is derived from the difference between two independently measured segment orientations. Since thorax–pelvis alignment is calculated from two separate IMU measurements, errors from both sensors are combined, which may result in a larger overall error.

Forward head posture (FHP) demonstrated the lowest accuracy among the four variables, with a mean RMSE of 2.012° and ICC of 0.799, along with the largest inter-subject variability (RMSE SD = 1.446°). This finding may be attributed to several factors. First, the head and cervical region involve smaller movement amplitudes compared with the pelvis and thorax, making the signal-to-noise ratio lower and measurement errors proportionally more significant. Second, FHP is calculated from two sensors: one on the head and one around C7. This means that errors from both sensors can be added together. Third, considerable inter-subject variability was

observed, particularly for S03, whose FHP R^2 value of 0.343 was markedly lower than the other participants. This outlier result may reflect individual differences in head movement strategy, cervical muscle tension, or variability in sensor placement between trials [26].
The RMSE values observed in this study for pelvic tilt, thorax tilt, and thorax–pelvis alignment were within the low-degree error range reported in previous IMU validation studies for spinal and trunk motion measurements. For example, Chang et al. reported RMSE values of 0.86–1.90° for through-range lumbar flexion measurements using DorsaVi IMUs compared with Vicon [40]. This suggests that the accuracy achieved in the present study is comparable to previous IMU-based motion analysis research and supports the feasibility of IMU-based sagittal posture monitoring, particularly for pelvic and thoracic measurements. However, clinical acceptability should still be interpreted with caution, as acceptable error depends on the specific posture variable, task, and intended application.

5.1.2 Comparison of Euler-Angle and Quaternion Methods

The comparison between Euler-angle–based and quaternion-based orientation representation methods revealed negligible differences in sagittal tilt estimation under the experimental conditions evaluated. Mean absolute differences between the two methods were below 0.5° for all posture tasks, with standard deviations below 0.56°. These results suggest that both methods produce functionally equivalent estimates for quasi-static sagittal posture assessment within the angular ranges tested.
The theoretical advantages of quaternion-based representations, including the avoidance of gimbal lock singularities and improved numerical stability during large or rapid rotations [34], did not translate into measurable performance differences under the current experimental conditions. This is likely because the posture tasks evaluated involved primarily uniplanar sagittal motion within moderate angular ranges, conditions under which Euler-angle representations are not expected to exhibit significant numerical instability.
The largest instantaneous differences between the two methods were observed during rapid motion transitions, with maximum differences reaching up to 4.95° for pelvic tilt. These transient discrepancies are consistent with the known sensitivity of Euler-angle representations to rapid multi-axis rotations, during which the sequential rotation decomposition may introduce brief numerical artefacts [34]. However, given that these differences were transient and did not persist during sustained posture holds, their practical impact on rehabilitation posture assessment is likely minimal.
From a practical standpoint, Euler-angle–based representations offer the advantage of direct clinical interpretability, as the computed angles correspond to anatomically meaningful rotation axes. For rehabilitation applications where clinicians require intuitive angle readouts, Euler-angle methods may therefore be easier to interpret. However, quaternion-based representations are more suitable for numerical computation, as they avoid gimbal lock and provide a more stable representation of orientation during continuous rotation. Therefore, although both methods produced comparable sagittal tilt estimates in the present quasi-static tasks, quaternion-based

methods may be preferred for algorithm implementation, signal processing, and applications involving larger angular ranges or more complex multi-planar movements [36].

5.1.3 Influence of Deep Breathing on Thorax Tilt Estimation

Visual inspection of the thorax tilt signals during deep breathing revealed periodic oscillations in both IMU and MoCap measurements across participants. These oscillations are consistent with rhythmic thoracic motion associated with respiration. Despite these oscillations, ICC values remained high for all participants (range: 0.993–0.998), indicating that the temporal pattern of thorax tilt was consistently tracked by the IMU system during deep breathing.

The RMSE values during deep breathing showed noticeable inter-subject variability, ranging from 0.55° to 2.63°. This variability may be related to differences in breathing amplitude, thoracic expansion pattern, sensor attachment stability, or soft-tissue motion around the thorax. Participants with larger respiratory-induced thoracic motion may produce greater local deformation at the sensor attachment site, which could increase the difference between IMU-based estimates and the MoCap marker-based reference. This may explain why S01 and S02 showed higher RMSE values and more visible offsets between the IMU and MoCap signals during the sustained forward thorax inclination posture.

These results suggest that deep breathing can introduce visible oscillatory components into thorax-mounted IMU signals during posture assessment. Therefore, respiratory motion should be considered when interpreting thorax tilt measurements, particularly when the posture is held for several seconds or when the participant breathes deeply during the measurement. In rehabilitation-related posture assessment, standardising breathing instructions may help improve measurement consistency, for example by asking participants to breathe normally or to avoid exaggerated deep breathing during static posture measurements.

It is important to acknowledge a methodological limitation in this analysis. Since MoCap markers were placed directly on the IMU attachment straps, both systems were affected by respiratory soft-tissue displacement at the sensor attachment region. Consequently, the RMSE values reported here reflect differences between the IMU-based estimates and the MoCap marker-based reference, rather than the absolute measurement error of the IMU system relative to true skeletal thorax orientation.

5.2 Part B: IMU-Based Respiration Monitoring

The results demonstrated that IMU-based respiratory signal extraction was feasible under deep breathing conditions, but showed limited reliability during normal breathing. During deep breathing, Pearson r values ranged from 0.803 to 0.964 (standing) and from 0.881 to 0.960 (sitting), indicating moderate to strong agreement. During normal breathing, agreement was considerably lower and more variable, with Pearson r ranging from 0.406 to 0.700.

The superior performance during deep breathing is consistent with the signal processing approach employed in this study, which extracted respiratory information from the relative orientation between anterior and posterior thoracic IMUs. Deep breathing produces larger thoracic expansion amplitudes, generating a stronger and more clearly detectable orientation change signal [38]. During normal breathing, the smaller amplitude of thoracic motion results in a lower signal-to-noise ratio, making it more difficult to reliably extract the respiratory component [41].
Body position had minimal influence on signal quality, with standing and sitting results showing similar agreement for most participants. This suggests that the approach is robust to postural context, which is practically relevant for rehabilitation applications where patients may need to be monitored across different postures. Considerable inter-subject variability was observed, particularly during normal breathing. This may be explained by differences in individual breathing patterns, including breathing rhythm, amplitude, and the relative contribution of thoracic versus abdominal motion. As a result, the respiratory signal captured by the thorax-mounted IMUs varied between participants, leading to subject-dependent agreement with the belt reference. [42].
Overall, IMU-based respiration monitoring using relative thoracic orientation is feasible for detecting deep breathing patterns, but may not be sufficiently reliable for clinical monitoring during normal tidal breathing without further refinement of the signal extraction approach. Future work could explore adaptive filtering strategies or machine learning-based approaches to improve respiratory signal extraction under low-amplitude breathing conditions [42].

5.3 General Limitations

Several limitations of this study should be acknowledged.
First, the sample size was small, with only four participants included in the posture assessment experiments and three in the respiration monitoring analysis. This limits the statistical power of the findings and the generalisability of the results to broader populations. Future studies with larger and more diverse participant samples, including individuals with musculoskeletal conditions, are needed to validate the findings in clinically relevant populations.
Second, all participants were healthy young adults, and the experimental tasks were performed under controlled laboratory conditions. The accuracy and reliability of IMU-based posture estimation in clinical rehabilitation populations, who may exhibit abnormal movement patterns, muscle weakness, or pain-related compensatory strategies, remains to be established.
Third, the methodological limitation regarding MoCap marker placement during breathing trials is discussed in detail in Section 5.1.3.
Fourth, the study evaluated only sagittal-plane posture variables. Multi-planar posture assessment, including frontal and transverse plane components, may present additional challenges for IMU-based systems and was not addressed in this work.
Finally, the respiration monitoring analysis was based on a limited number of trials and participants. Future work should include more participants and repeated

measurements to better evaluate the reliability of IMU-based respiration monitoring across different breathing patterns and body positions.

6
Conclusion

This chapter summarises the main findings of the thesis, outlines the contributions of the work, and suggests directions for future research.

6.1 Summary of Findings

Part A of this thesis investigated the accuracy, reliability, and robustness of IMU-based sagittal posture estimation for rehabilitation-related applications. The study focused on pelvic tilt, thorax tilt, thorax–pelvis relative alignment, and forward head posture, and additionally evaluated the influence of orientation representation methods and deep breathing on measurement performance.
IMU-based sagittal posture estimation demonstrated good agreement with the MoCap reference system across most posture variables. Pelvic tilt achieved the highest accuracy and repeatability, followed by thorax tilt and thorax–pelvis alignment. Forward head posture showed lower agreement and greater inter-subject variability compared with the other posture variables.
The comparison between Euler-angle–based and quaternion-based orientation estimation methods revealed only minor differences under the evaluated experimental conditions. Both methods produced highly comparable sagittal tilt estimates for the quasi-static posture tasks investigated in this study.
Deep breathing introduced visible oscillations into thorax-mounted IMU signals. Despite this effect, overall IMU–MoCap agreement remained high during breathing tasks.
Part B of this thesis explored the feasibility of IMU-based respiration monitoring using relative thoracic orientation.
IMU-based respiration monitoring demonstrated moderate to strong agreement with the respiratory belt reference during deep breathing, but lower and more variable agreement during normal breathing. These findings suggest that IMU-derived respiratory signal extraction is feasible under controlled conditions, although further development is required for reliable normal-breathing monitoring.
Overall, the findings of this thesis support the feasibility of IMU-based sagittal posture assessment for rehabilitation-related applications, particularly for pelvic and thoracic posture monitoring.

6.2 Contributions

The main contributions of this thesis are as follows:

- Validation of IMU-based sagittal posture estimation against a MoCap reference system across multiple clinically relevant posture variables.
- Comparison of Euler-angle–based and quaternion-based orientation representations for sagittal posture assessment.
- Investigation of the influence of respiratory motion on thorax-mounted IMU posture measurements.
- Exploratory evaluation of IMU-based respiration monitoring using relative thoracic orientation.

6.3 Future Work

Future work should include larger and more diverse participant groups, including clinical rehabilitation populations, to further evaluate the robustness and clinical applicability of IMU-based posture assessment. Additional research is also needed to improve breathing-related artefact suppression and develop more robust respiratory signal extraction methods for normal breathing conditions.
Another potential direction is the integration of plantar pressure and foot load distribution measurements with IMU-based sagittal posture assessment. Plantar loading patterns are closely related to whole-body sagittal alignment and load transfer, and such integration could provide a more comprehensive assessment framework for rehabilitation applications.

Declaration of AI Tool Usage

During the preparation of this thesis, artificial intelligence (AI) tools were used for literature retrieval and reading, idea generation, language refinement, grammar correction, structural organisation, and LaTeX formatting support. AI tools were also used for programming assistance and debugging support during code development. All research design, experimental setup, data collection, data processing, analysis, interpretation of results, and scientific conclusions were conducted and verified by the author. AI tools were not used to generate experimental data or perform scientific analysis independently.
The author takes full responsibility for the content and accuracy of this thesis.

Bibliography

[1] G. Stucki, J. Bickenbach, C. Gutenbrunner, and J. L. Melvin, "Rehabilitation: The health strategy of the 21st century," *Rehabilitation*, vol. 4, pp. 18–20, 2018.

[2] A. Petropoulos, D. Sikeridis, and T. Antonakopoulos, "Spomo: IMU-based real-time sitting posture monitoring," in *2017 IEEE 7th International Conference on Consumer Electronics – Berlin (ICCE-Berlin)*, p. 59, 2017.

[3] C. Krauter, K. Angerbauer, A. S. Calepso, A. Achberger, S. Mayer, and M. Sedlmair, "Sitting posture recognition and feedback: A literature review," in *Proceedings of the CHI Conference on Human Factors in Computing Systems*, vol. 120, 2024.

[4] S. B. O'Sullivan, T. J. Schmitz, and G. Fulk, *Physical Rehabilitation*. FA Davis, 2019.

[5] A. Cieza, "Rehabilitation: the health strategy of the 21st century, really?," *Archives of Physical Medicine and Rehabilitation*, vol. 100, no. 11, pp. 2212–2214, 2019.

[6] D. Czaprowski, Stoliński, M. Tyrakowski, M. Kozinoga, and T. Kotwicki, "Non-structural misalignments of body posture in the sagittal plane," *Scoliosis and Spinal Disorders*, vol. 13, no. 1, 2018.

[7] C. M. Lind, "A rapid review on the effectiveness and use of wearable biofeedback motion capture systems in ergonomics to mitigate adverse postures and movements of the upper body," *Sensors*, vol. 24, no. 11, p. 3345, 2024.

[8] R. A. Laird, J. Gilbert, P. Kent, and J. L. Keating, "Comparing lumbo-pelvic movement in people with and without back pain: A systematic review," *BMC Musculoskeletal Disorders*, vol. 15, pp. 1–13, 2014.

[9] S. J. Preece, P. Willan, C. J. Nester, P. Graham-Smith, L. Herrington, and P. Bowker, "Variation in pelvic morphology may prevent the identification of anterior pelvic tilt," *Journal of Manual & Manipulative Therapy*, vol. 16, no. 2, pp. 113–117, 2008.

[10] T. Sugavanam, R. Sannasi, P. A. Anand, and P. A. Javia, "Postural asymmetry in low back pain: A systematic review and meta-analysis of observational studies," *Disability and Rehabilitation*, vol. 47, no. 7, pp. 1659–1676, 2025.

[11] Y. Yarayan and Şevgin, "Association of thoracic kyphosis angle with shoulder pain, range of motion, isokinetic muscle strength, and upper extremity function," *BMC Musculoskeletal Disorders*, vol. 27, p. 255, 2026.

[12] F. Binaei, A. H. Kahlaee, C. T. Delkhoush, N. Rahmani, M. A. M. Bandpei, and M. Saatchi, "The correlation between pain and flexor and extensor muscle endurance and size with craniovertebral angle changes during prolong sitting

task," *Journal of Bodywork and Movement Therapies*, vol. 45, pp. 400–405, 2025.

[13] A. A.-O. X. Alghadir and Z. A.-O. Iqbal, "Effect of deep cervical flexor muscle training using pressure biofeedback on pain and forward head posture in school teachers with neck pain: An observational study," *BioMed Research International*, vol. 2021, 2021.

[14] A. Cieza, K. Causey, K. Kamenov, S. W. Hanson, S. Chatterji, and T. Vos, "Global estimates of the need for rehabilitation based on the Global Burden of Disease Study 2019: a systematic analysis for the Global Burden of Disease Study 2019," *The Lancet*, vol. 396, no. 10267, pp. 2006–2017, 2020.

[15] J. Z. Edwards, K. A. Greene, R. S. Davis, M. W. Kovacik, D. A. Noe, and M. J. Askew, "Measuring flexion in knee arthroplasty patients," *The Journal of Arthroplasty*, vol. 19, no. 3, pp. 369–372, 2004.

[16] A. Tognetti, F. Lorussi, N. Carbonaro, and D. D. Rossi, "Wearable goniometer and accelerometer sensory fusion for knee joint angle measurement in daily life," *Sensors*, vol. 15, no. 11, pp. 28435–28455, 2015.

[17] M. P. D. Looze, H. M. Toussaint, J. Ensink, C. Mangnus, and A. J. V. D. Beek, "The validity of visual observation to assess posture in a laboratory-simulated manual material handling task," *Ergonomics*, vol. 37, no. 8, pp. 1335–1343, 1994.

[18] X. Fan, D. Xue, Z. Pan, and Y. Wang, "Comparison of sagittal spinal alignment on standing plain X-Rays and supine MRI in degenerative lumbar disease," *Frontiers in Surgery*, vol. 10, p. 1103952, 2023.

[19] U. G. Longo, S. D. Salvatore, A. Carnevale, S. M. Tecce, B. Bandini, A. Lalli, E. Schena, and V. Denaro, "Optical motion capture systems for 3D kinematic analysis in patients with shoulder disorders," *International Journal of Environmental Research and Public Health*, vol. 19, no. 19, p. 12033, 2022.

[20] D. A. Szabo, N. Neagu, S. Teodorescu, M. Apostu, C. Predescu, C. Pârvu, and C. Veres, "The role and importance of using sensor-based devices in medical rehabilitation: A literature review on the new therapeutic approaches," *Sensors*, vol. 23, no. 21, p. 8950, 2023.

[21] L. Simpson, M. M. Maharaj, and R. J. Mobbs, "The role of wearables in spinal posture analysis: A systematic review," *BMC Musculoskeletal Disorders*, vol. 20, 2019.

[22] N. K. M. Yoong, J. Perring, and R. J. Mobbs, "Commercial postural devices: A review," *Sensors*, vol. 19, p. 5128, 2019.

[23] T. Seel, J. Raisch, and T. Schauer, "IMU-based joint angle measurement for gait analysis," *Sensors*, vol. 14, no. 4, pp. 6891–6909, 2014.

[24] Y. Zheng, K. C. Chan, and C. C. L. Wang, "Pedalvatar: An IMU-based real-time body motion capture system using foot-rooted kinematic model," in *Proceedings of the 2014 IEEE/RSJ International Conference on Intelligent Robots and Systems (IROS)*, (Chicago, IL, USA), pp. 4130–4135, 2014.

[25] D. Paloschi, M. Bravi, E. Schena, S. Miccinilli, M. Morrone, S. Sterzi, P. Saccomandi, and C. Massaroni, "Validation and assessment of a posture measurement system with magneto-inertial measurement units," *Sensors*, vol. 21, no. 19, p. 6610, 2021.

[26] R. Lee, R. Akhundov, C. James, S. Edwards, and S. J. Snodgrass, "Variations in concurrent validity of two independent inertial measurement units compared to gold standard for upper body posture during computerised device use," *Sensors*, vol. 23, no. 15, p. 6761, 2023.

[27] W. Y. Wong and M. S. Wong, "Trunk posture monitoring with inertial sensors," *European Spine Journal*, vol. 17, pp. 743–753, 2008.

[28] J. Xuan, T. Zhu, G. Peng, F. Sun, and D. Dong, "A review on the inertial measurement unit array of microelectromechanical systems," *Sensors*, vol. 24, no. 22, p. 7140, 2024.

[29] H. Chen, M. C. Schall Jr., and N. Fethke, "Effects of movement speed and magnetic disturbance on the accuracy of inertial measurement units," *Proceedings of the Human Factors and Ergonomics Society Annual Meeting*, vol. 61, no. 1, pp. 1046–1050, 2017.

[30] P. N. Pathirana, M. S. Karunarathne, G. L. Williams, *et al.*, "Robust and accurate capture of human joint pose using an inertial sensor," *IEEE Journal of Translational Engineering in Health and Medicine*, vol. 6, pp. 1–11, 2018.

[31] S. O. H. Madgwick, A. J. L. Harrison, and R. Vaidyanathan, "Estimation of IMU and MARG orientation using a gradient descent algorithm," in *Proceedings of the 2011 IEEE International Conference on Rehabilitation Robotics (ICORR)*, (Zurich, Switzerland), pp. 1–7, 2011.

[32] A. G. Quinchia, G. Falco, E. Falletti, F. Dovis, and C. Ferrer, "A comparison between different error modeling of MEMS applied to GPS/INS integrated systems," *Sensors*, vol. 13, no. 8, pp. 9549–9588, 2013.

[33] G. Welch and G. Bishop, "An introduction to the Kalman filter," tech. rep., University of North Carolina at Chapel Hill, 2006.

[34] J. H. Challis, "Quaternions as a solution to determining the angular kinematics of human movement," *BMC Biomedical Engineering*, vol. 2, no. 1, p. 5, 2020.

[35] G. Arnold, F. R. Sarlegna, L. G. Fernandez, and M. Auvray, "Somatosensory loss influences the adoption of self-centered versus decentered perspectives," *Frontiers in Psychology*, vol. 10, p. 419, 2019.

[36] K. Sygit *et al.*, "Time and frequency domain analysis of IMU-based orientation estimation algorithms with comparison to robotic arm orientation as reference," *Sensors*, vol. 25, no. 16, p. 5161, 2025.

[37] J. B. Kuipers, *Quaternions and Rotation Sequences: A Primer with Applications to Orbits, Aerospace, and Virtual Reality*. Princeton University Press, 1999.

[38] M. Ceccarelli, M. D'Onofrio, V. Ambrogi, and M. Russo, "An experimental evaluation of respiration by monitoring ribcage motion," *Applied Sciences*, vol. 13, no. 15, p. 8938, 2023.

[39] T. K. Koo and M. Y. Li, "A guideline of selecting and reporting intraclass correlation coefficients for reliability research," *Journal of Chiropractic Medicine*, vol. 15, no. 2, pp. 155–163, 2016.

[40] R. P. Chang, A. Smith, P. Kent, N. Saraceni, M. Hancock, P. B. O'Sullivan, and A. Campbell, "Concurrent validity of DorsaVi wireless motion sensor system Version 6 and the Vicon motion analysis system during lifting," *BMC Musculoskeletal Disorders*, vol. 23, no. 1, p. 909, 2022.

[41] R. D. Fazio, M. Stabile, M. D. Vittorio, R. Velázquez, and P. Visconti, "An overview of wearable piezoresistive and inertial sensors for respiration rate monitoring," *Electronics*, vol. 10, no. 17, p. 2178, 2021.

[42] A. Angelucci and A. Aliverti, "An IMU-based wearable system for respiratory rate estimation in static and dynamic conditions," *Cardiovascular Engineering and Technology*, vol. 14, no. 3, pp. 351–363, 2023.

A

Appendix 1

A.1 IMU-Based Posture Estimation Accuracy

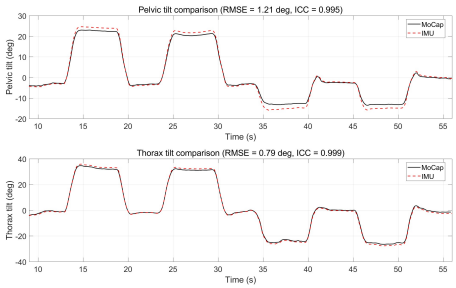

(a) Thorax forward and backward tilt

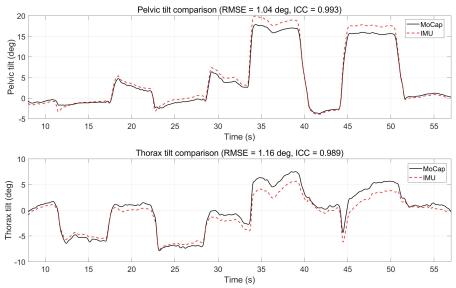

(b) Pelvic posterior and anterior tilt

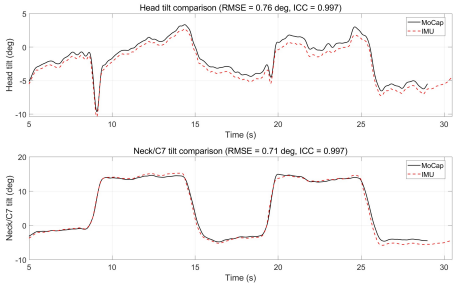

(c) Head tilt and neck tilt

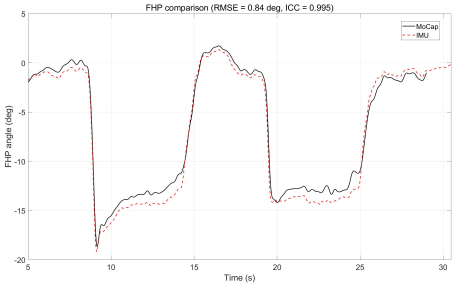

(d) Forward head posture (FHP)

Figure A.1: Time-series comparison between IMU (dashed red) and MoCap (solid black) posture estimates for participant S02.

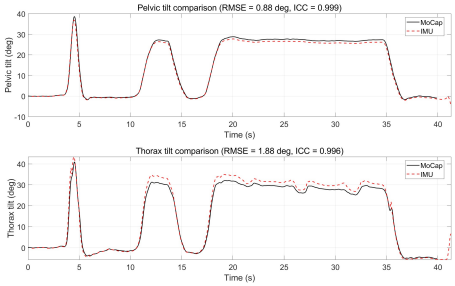

(a) Thorax forward and backward tilt

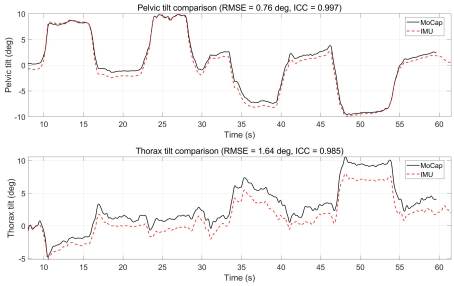

(b) Pelvic posterior and anterior tilt

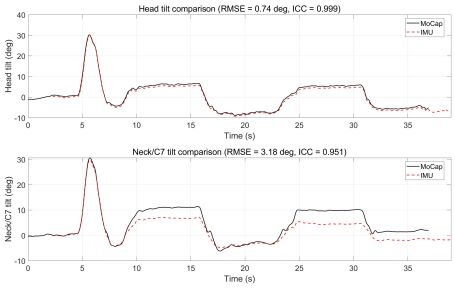

(c) Head tilt and neck tilt

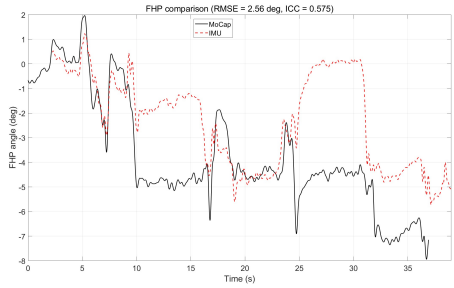

(d) Forward head posture (FHP)

Figure A.2: Time-series comparison between IMU (dashed red) and MoCap (solid black) posture estimates for participant S03.

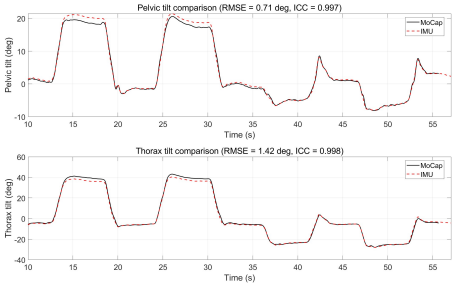

(a) Thorax forward and backward tilt

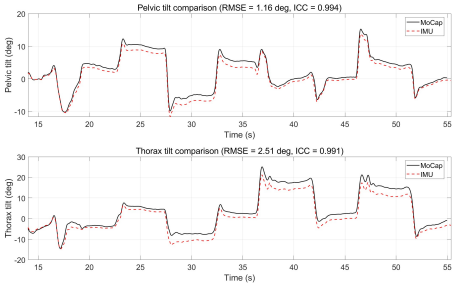

(b) Pelvic posterior and anterior tilt

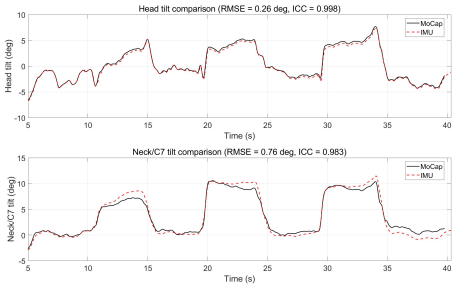

(c) Head tilt and neck tilt

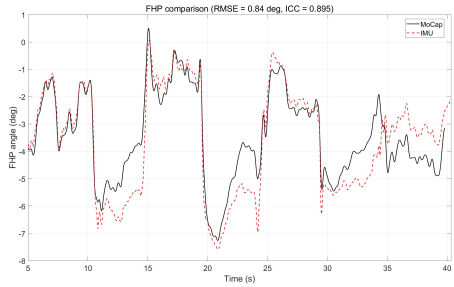

(d) Forward head posture (FHP)

Figure A.3: Time-series comparison between IMU (dashed red) and MoCap (solid black) posture estimates for participant S04.

DEPARTMENT OF ELECTRICAL ENGINEERING
CHALMERS UNIVERSITY OF TECHNOLOGY
Gothenburg, Sweden
www.chalmers.se

CHALMERS
UNIVERSITY OF TECHNOLOGY